14th World Congress in Computational Mechanics (WCCM)
ECCOMAS Congress 2020
19 – 24 July 2020, Paris, France
F. Chinesta, R. Abgrall, O. Allix and M. Kaliske (Eds)

APPLICATION OF THE MESHLESS METHOD FOR PHARMACOKINETIC PARAMETER IDENTIFICATION

ANTHONY M. KHOURY [1], VLADIMIR V. GOLUBEV[2] AND EDUARDO A. DIVO[3]

[1] Department of Mechanical Engineering – Embry-Riddle Aeronautical University
1 Aerospace Blvd. Daytona Beach, FL 32114, USA
E-mail: khourya@my.erau.edu

[2] Department of Aerospace Engineering – Embry-Riddle Aeronautical University
1 Aerospace Blvd. Daytona Beach, FL 32114, USA
E-mail: golubd1@erau.edu

[3] Department of Mechanical Engineering – Embry-Riddle Aeronautical University
1 Aerospace Blvd. Daytona Beach, FL 32114, USA
E-mail: divoe@erau.edu

Key words: Transdermal Drug Delivery, Meshless Method, Localized Collocation, Parameter Identification, Inverse Problems.

Abstract. The Localized Collocation Meshless Method (LCMM) is applied to the solution of a set of partial differential equations describing the diffusive transport of a dermally injected compound. This efficient and accurate numerical technique then provides the framework for the estimation of pharmacokinetic (PK) parameters by the comparison of two models, both containing information derived from experimental results, using the iterative Golden Section search algorithm. This comparison is quantified using a norm between the two solution spaces. While this method does provide an estimate of the effective-diffusion coefficient, it ultimately demonstrates that a simple, free-diffusion model is inadequate for quantifying the spatial and temporal distribution of a dermally-injected compound if elimination effects are not accounted for properly.

1 INTRODUCTION

Given the complexity of the skin structure, see Figure 1, there has been significant work in the characterization of the skin and its functionality, particularly as pertains to transdermal drug delivery (TDD) methods and systems. There are some typical simplifying assumptions and modeling methodologies that have been explored and validated to address some of these multiscale complexities[1]. For example, treating a skin layer as a homogenous medium, first-order loss mechanisms, partitioning effects, etc[1–4]. In their 2008 work describing the diffusivity of skin permeants, Kretsos et al. outlined a regression-analysis based approach for the determination of coefficients that describe the transport of dermis-injected substances[5].

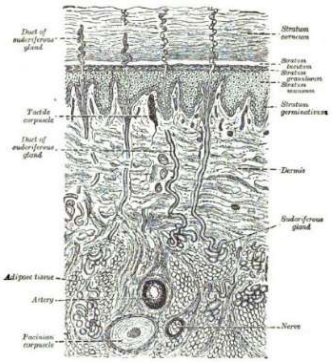

Figure 1: Skin Cross Section[6]

Here, the authors apply the Localized Collocation Meshless Method (LCMM) to the solution of a Fickian or diffusion-based pharmacokinetic model layers[2,5,7,8]. The advantages afforded by the LCMM provide an efficient framework for characterizing the transport behavior of permeants of interest. First, the LCMM allows for modeling the forward problem of quantifying the transport phenomenon of a compound delivered by injection into the dermis. This then gives way to the inverse problem of parameter estimation by identifying diffusion coefficients that characterize the rate at which this transport occurs.

Thus, the need arises for several themes to be outlined. First, the PK model defining the transport behavior of a dermis-injected substance. Second, and of primary importance to this work is the numerical modeling strategy, the LCMM. Finally, the inverse method will be addressed in brief, describing the process by which a diffusion coefficient is found.

2 TRANSDERMAL COMPOUND TRANSPORT MODEL

In modeling the transport of a compound in the dermis, there are several multi-scale, biophysical effects to be considered, including adsorption[1,2,9,10], partitioning[3,11], metabolic reactions[7,12,13], and elimination[1,4,5]. Following prior work, an extension of Fick's second law is implemented to account for these various biophysical effects[1,2,10,11].

2.1 Two-Compartment Model

Following prior work, an extension of Fick's second law is implemented to account for these various biophysical effects[1,2,10,11]. The one-dimensional flux per unit area, J, of a substance transported by diffusion within a solvent follows Fick's first law, given as:

$$J = -D\frac{\partial c}{\partial x} \tag{1}$$

Where: D - diffusion coefficient $[m^2 / s]$ and

c - compound concentration in tissue compartment $[kg / m^3]$

Considering storage effects, that is, conservation of mass of the transported solute, one arrives at the one-dimensional transient diffusion equation, known as Fick's second law:

$$\frac{\partial c}{\partial t} = D\frac{\partial^2 c}{\partial^2 x} \tag{2}$$

This then defines the diffusion of the compound in the tissue compartment. To account for the second compartment, here, the blood domain, adsorption effects need to be considered. This is accomplished by assuming linear coupling between the substance concentrations that are bound to the tissue and blood compartments respectively; accomplished by a binding rate coefficient, normalized by the volume of the compartments to account for mass-balance[9,11,12]. This introduces a second equation quantifying the storage of the compound in the blood compartment such that:

$$\frac{\partial c}{\partial t} = D\frac{\partial^2 c}{\partial^2 x} + (\nu_b K_{12} c_b -_t K_{21} c) \tag{3}$$

$$\frac{\partial c_b}{\partial t} = (\frac{1}{\nu_b} K_{21} c - K_{12} c_b) \tag{4}$$

Where: c_b - compound concentration in blood compartment $[kg/m^3]$

ν_b - volume ratio, where: $\nu_b = V_b / V_t = 0.1$ [14]

V_t, V_b - volume of tissue and blood compartments $[m^3]$

K_{12}, K_{21} - binding and unbinding rate coefficients $[1/s]$

Additionally, there exist clearance effects such as metabolism and elimination which result in the active removal of the compound from the tissue and blood compartments, respectively. These clearance effects are typically accounted for using first-order processes[4,5,7,9,12,15]. Anissimov et al. suggest that the elimination rate constant is proportional to the blood flow rate per unit volume of dermis, q_b [3,9,16]. These final effects result in the following addendums to the governing equations:

$$\frac{\partial c}{\partial t} = D\frac{\partial^2 c}{\partial^2 x} + (\nu_b K_{12} c_b -_t K_{21} c) - K_m c \tag{5}$$

$$\frac{\partial c_b}{\partial t} = (\frac{1}{\nu_b} K_{21} c - K_{12} c_b) - K_e c_b \tag{6}$$

Where: K_m, K_e - metabolic and elimination rate coefficients $[1/s]$

2.2 Simple Diffusion

It is suggested by Kretsos et al. that there exists a "free diffusivity" coefficient, D_{free}, that describes the *freely* diffusing concentration of a compound, c_{free} [5]. This is juxtaposed to the total concentration in the dermis, c_{de}, which is subject to partitioning and binding. This is effectively what is modeled in the above equations, given in equation (5) by the variable c, the concentration in the dermis; which can be bound, metabolized and adsorbed by the blood. In their work, an equation for the free diffusion coefficient, D_{free}, in units of $[cm^2/s]$, is

given as a function of molecular weight (MW) given in units of Daltons $[Da]$,where[5]:

$$\log D_{free} = -4.15 - 0.655 \log MW \tag{7}$$

This equation was extracted from a data reduction technique using results from various studies of physicochemical properties and pharmacokinetic parameters of selected compounds in mammalian dermis, primarily *in vitro* steady-state flux experiments[5]. The data collected for these experiments in mammalian dermis demonstrate a close correlation between the free diffusivity of a compound and its molecular weight, when neglecting the data from Tojo et al., indicated by the empty diamonds[17]. It is speculated that the differences in the data reported by Tojo et al. are caused by the methods in which the dermis was prepared[5,17].

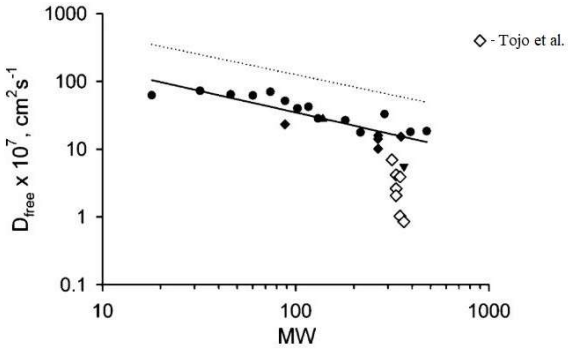

Figure 2: Free Diffusivity $[cm^2 / s]$ versus Molecular Weight $[Da]$[5]

However, this free diffusion coefficient results in a slightly modified representation of the concentration field. Again, this free diffusion coefficient represents the transport of "freely diffusing" compound concentration and does not consider effects such as binding and partitioning[5]. Such a model would then take on the form:

$$\frac{\partial c}{\partial t} = D_{free} \nabla^2 c \tag{8}$$

By providing an estimate for a free diffusion coefficient, this allows numerical methods to identify other pharmacokinetic coefficients when only partial data exists for the total diffusion of a compound. This is the approach takin herein, where the free diffusion coefficient will supplement existing experimental data for partitioning coefficients and the like, such that the effective diffusion coefficient can be deduce inversely. Before such an effort can be undertaken, an appropriate modeling method must be established.

3 MESHLESS METHOD

The Localized Collocation Meshless Method is a numerical technique for the solution of partial differential equations (PDE's), derived from an interpolation strategy utilizing radial-basis functions (RBF)[18–20]. This method has several inherent benefits that make it preferable to traditional modeling techniques [19–23]. This is especially true in inverse problems, where

the iterative nature of the solution methods can leverage the pre-computing strategy of derivative interpolators in the localized method[24–26].

3.1 Domain Definition

To begin, consider any generic domain, Ω, circumscribed by the boundary, Γ. This formulation defines a set of NC data centers. A number of these are distributed within the domain, NI interior data centers, and a number restricted to the boundary, NB boundary data centers; where governing equations are applied to the former while boundary conditions to the latter. Note that there is no requirement for a regular or structured distribution of the data centers, given the implementation of radial-basis functions (RBF), which are supported on the global domain[18,27–29].

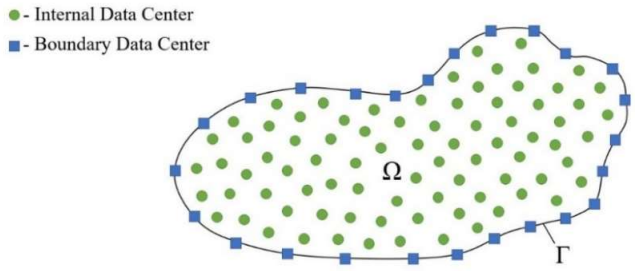

Figure 3: Generalized 2D Meshless Domain, Ω, with Boundary Γ

3.2 Local Expansion

For illustration, consider a general field variable in a generalized time and space coordinate system, $\phi(x,t)$, governed by an equation such as that of free diffusion given in equation 8, with an arbitrary diffusion coefficient, D. This field variable and governing equation are valid over the domain, Ω.

$$\frac{\partial \phi(x,t)}{\partial t} = D\nabla^2 \phi(x,t) \tag{9}$$

While governing equation is valid over the domain, there is also a generalized boundary condition for the field variable, $\phi(x,t)$, specified on the boundary, Γ, such that:

$$\hat{\beta}_1 \frac{\partial \phi}{\partial n} + \hat{\beta}_2 \phi = \hat{\beta}_3 \tag{10}$$

This generalized boundary condition allows one t dictate the boundary condition type and constrain values by imposing the coefficients, $\hat{\beta}_1, \hat{\beta}_2$ and $\hat{\beta}_3$.

In the LCMM, a localized linear expansion is sought over a topology or group of influence points around each data center, such that each topology contains NF influence points. This expansion takes the form:

$$\phi(x) = \sum_{j=1}^{NF} \alpha_j \chi_j(x) + \sum_{j=1}^{NP} \alpha_{j+NF} P_j(x) \tag{10}$$

In this expansion, $\chi_j(x)$ are pre-defined functions chosen from the family of Radial-Basis Functions (RBF), given their favorable convergence criteria and proven performance in interpolation schemes[20–22]. These expansion functions are augmented by number of *NP* polynomial functions, $P_j(x)$, to guarantee the exact retrieval of constant and linear solutions. The expansion coefficients, α_j, are as of yet unknown, but will be quantified at each time level, as they evolve with the solution over time. Here, the inverse multiquadric RBF is selected and is given such that:

$$\chi_j(x) = \left[r_j^2(x) + \sigma^2 \right]^{n-\frac{3}{2}} \tag{11}$$

Where n is any positive exponent, here $(n=1)$, σ is a shape parameter and $r_j(x)$ is the radial distance defined in the 2D Cartesian coordinate system as:

$$r_j(x) = \sqrt{\left(x - x_j\right)^2 + \left(y - y_j\right)^2} \tag{12}$$

To solve for the field variable, ϕ, at the current time step, one begins with the known field solution from the time step prior. This known field solution is then collocated at points within the localized topology, resulting in the following set of equations given in matrix-vector form:

$$\{\phi\} = [C]\{\alpha\} \tag{13}$$

Where the left-hand side known vector is given as:

$$\{\phi\} = \begin{Bmatrix} \phi(x_1) \\ \vdots \\ \phi(x_{NF}) \\ 0 \\ \vdots \\ 0 \end{Bmatrix} \tag{14}$$

And the resulting collocation matrix defining the system of equations is given by:

$$[C] = \begin{bmatrix} \chi_1(x_1) & \cdots & \chi_{NF}(x_1) & P_1(x_1) & \cdots & P_{NP}(x_1) \\ \vdots & \ddots & \vdots & \vdots & \ddots & \vdots \\ \chi_1(x_{NF}) & \cdots & \chi_{NF}(x_{NF}) & P_1(x_{NF}) & \cdots & P_{NP}(x_{NF}) \\ P_1(x_1) & \cdots & P_1(x_{NF}) & 0 & \cdots & 0 \\ \vdots & \ddots & \vdots & \vdots & \ddots & \vdots \\ P_{NP}(x_1) & \cdots & P_{NP}(x_{NF}) & 0 & \cdots & 0 \end{bmatrix}_{NF+NP,NF+NP} \tag{15}$$

Note that this collocation matrix is unique to each topology and is dependent *explicitly* on the geometrical distribution of the data centers within said topology, and thus, can be calculated at the setup stage to then be implemented at all time steps.

Finally, the expansion coefficients, α_j, are determined such that:

$$\{\alpha\} = [C]^{-1}\{\phi\} \tag{16}$$

Noting the inversion of the collocation matrix, the selection of this shape parameter, σ, is far from arbitrary; varying the shape parameter *does* improve the solution accuracy[21,22,27]. As the shape parameter increases, the interpolation becomes smoother and more accurate. However, this causes the collocation matrix to tend towards numerically-singular as the elements of $[C]$ become dominated by the shape factor and sets within the matrix begin to lose linear independence[24,30–32]. Following Cheng, a simple optimization scheme is implemented to maximize the shape parameter on each topology, to improve accuracy, until the condition number of the collocation matrix is in the range of 10^{11}-10^{12}[26,27].

3.3 On Efficiency

Meshless techniques utilizing RBF, particularly multiquadric RBF, benefit from spectral convergence in globally collocated methods[19,33]. Although the claim to spectral convergence is lost in localized collocation, local methods are less susceptible to ill-conditioning without the expense of domain decomposition and still retains a degree of accuracy unmatched by traditional meshed methods[23,24,30].

However, the real advantage of the localized method is the manner in which derivatives of the field variable are calculated at the data centers of each topology, x_c. Take, for instance, any linear differential operator, L, to be applied over the field variable, valid on the domain under consideration. This differential operator can be applied over the localized expansion quite simply as:

$$L\phi(x_c) = \sum_{j=1}^{NF} \alpha_j L\chi_j(x_c) + \sum_{j=1}^{NP} \alpha_{j+NF} LP_j(x_c) \tag{17}$$

As the expansion and polynomial functions have been defined *a priori*, then the derivatives of these functions can be defined explicitly. Denoting the field variable derivative at a data center, $L\phi(x_c)$, as, $L\phi_c$ this can be written in matrix-vector form as:

$$L\phi_c = \{L_c\}^T \{\alpha\} \tag{18}$$

Where:

$$\{L_C\} = \begin{bmatrix} L\chi_1(x_c) \\ \vdots \\ L\chi_{NF}(x_c) \\ LP_1(x_c) \\ \vdots \\ LP_{NP}(x_c) \end{bmatrix}_{NF+NP,1} \tag{19}$$

The expansion coefficients, $\{\alpha\}$, can be substituted into this definition, having been defined in equation 16 such that:

$$L\phi_c = \{L_c\}^T [C]^{-1} \{\phi\} \tag{20}$$

Casting the product of the expansion function derivates, $\{L_c\}^T$, with the inverse of the collocation matrix, $[C]^{-1}$, as:

$$\{L\}^T = \{L_c\}^T [C]^{-1} \tag{21}$$

Then the field derivatives can be reduced to:

$$L\phi_c = \{L\}^T \{\phi\} \tag{22}$$

The vector $\{L\}_{NF,1}$ directly interpolates the derivative of the field variable, ϕ, at the data center, x_c, of each topology. Like the collocation matrix, this is dependent entirely on the geometry of the topology and so be pre-computed and stored for later use. This derivative interpolation definition can be applied to *any* derivative operator valid on the space, such as a simple 1D spatial derivative, $\partial\phi/\partial x$, to something more complex such as the Laplace operator seen in diffusion equations, $\nabla^2\phi$, even in higher dimensional problems. Rather than calculating derivatives with finite-differencing approximations and the concerns of spatial resolution, derivatives are quantified explicitly here and with greater accuracy, given the interpolation accuracy[20]. Additionally, the pre-built derivative interpolation vectors save considerably computation time over the course of the solution, especially in applications when a solution might be sought repeatedly, such as in inverse schemes.

3.4 Time Marching

Given the form of the governing equations approximates:

$$\frac{\partial\phi}{\partial t} = D\nabla^2\phi \tag{23}$$

Then an explicit, first-order finite-differencing scheme can be implemented to advance the solution at the data centers, such that:

$$\phi_c^{k+1} = \phi_c^{k+1} + D\Delta t(\nabla^2\phi_c^k) \tag{24}$$

Where the superscript, k, indicates the time level of the solution and Δt is the time step by which the solution advances.

4 PARAMETER IDENTIFICATION: AN INVERSE TECHNIQUE

As stated prior, Kretsos poses a mathematical relation between the free diffusion of a substance within the dermis and the molecular weight of the substance as seen above in equation 7[5]. By neglecting elimination effects and the bound mass of the substance in other compartments implies the simplified compound transport reported in equation 8. However, the transport of a compound in the tissue can be more fully represented by the two-compartment model given as:

$$\frac{\partial c}{\partial t} = D_{eff}\frac{\partial^2 c}{\partial^2 x} + (\nu_b K_{12} c_b -_t K_{21} c) \tag{25}$$

$$\frac{\partial c_b}{\partial t} = (\frac{1}{\nu_b} K_{21} c - K_{12} c_b) \tag{26}$$

In many cases, the difficulties posed by measuring compound concentrations *in vivo*, leads to less reliable quantifications of D_{eff} in the dermis. However, other pharmacokinetic parameters can be extrapolated readily by observing systemic effects[9,34–36].

Thus, the motivation to inversely identify D_{eff} using numerical methods. This endeavor is made possible by: (a) the availability of other PK parameters in existing literature and (b) the free diffusion model against which the total or effective diffusion can be compared.

4.1 Numerical Domain

The free diffusion and effective diffusion equations are modeled on the same domain, given in Figure 4. This domain is 1 cm in width with a depth of approximately 1200 μm, the average depth of the dermis and epidermis in facial tissue, a region of interest for the authors' future work[37]. This domain begins with an initial concentration of 30 mg/mL having been injected by a 33 gauge needle into the dermal layers, as shown in Figure 4, and is allowed to diffuse through the dermis over an 8 hour time period. The data centers are distributed throughout this domain with an average spacing of approximately 0.01 cm.

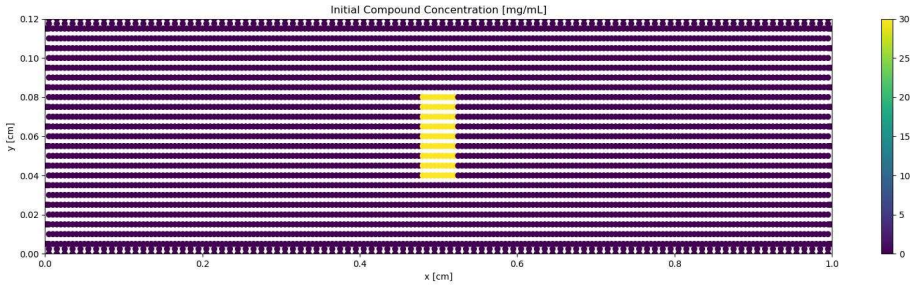

Figure 4: Initial Compound Concentration

The inverse method is applied to the identification of the effective diffusion coefficient of verapamil, for which the PK coefficients are readily available. The PK coefficients for verapamil are as follows:

Table 1: Verapamil PK Coefficients

Parameter	Value	Units	Parameter	Value	Units
MW	454.6	Da	K_e	$5 \cdot 10^{-3}$	$1/s$
D_{free}	$1.067 \cdot 10^{-6}$	cm^2/s	K_{12}	$2.19 \cdot 10^{-4}$	$1/s$
K_m	$5.61 \cdot 10^{-4}$	$1/s$	K_{21}	$1.11 \cdot 10^{-4}$	$1/s$

4.2 PID: Golden Section Search

The problem of inversely identifying the effective diffusion coefficient is one of minimization, that is, of minimizing the distance between the free diffusion solution and the effective diffusion solution. The two solution spaces can be sampled at the same points in time and space and compared using the L_2-norm to quantify the distance between the results[38]. Given some measurements from the free diffusion model, c_{free}, and effective diffusion model, c_{eff}, then the L_2-norm is calculated such that[25]:

$$L_2 = \sqrt{\frac{1}{N}\sum_{i=1}^{N}\left[c_{free}(x_i, y_i, t_i) - c_{eff}(x_i, y_i, t_i)\right]^2} \tag{24}$$

Whereby N is the number of sampled points from the field solutions. This objective function we seek to minimize is essentially 1D and presumably unimodal by definition, there will be one value for D_{eff} that will create a spatial distribution most similar to that returned by the free-diffusion model. However, there is no analytical relationship between the objective function and the design parameter, D_{eff}, that is readily available for analytical or gradient-based approaches. Thus, the Golden Section search algorithm is implemented for this minimization[39]. Golden Section search is technique similar to bisection; it evaluates the objective function at two locations and attempts to determine a bound on the domain within which the minimum exists.

The search is fairly efficient; given a range within which the parameter exists, this method reduces this range by approximately 32% on each iteration. This means that in 10 iterations, the Golden Section search will have a ruled about 99.2% of the initial bounds within which the solution belongs to. That is, if one predicts that the value for D_{eff} falls within the range of $[0,100]\ cm^2/s$, within 10 iterations, this method will narrow down the selection to a range of $0.813\ cm^2/s$. Here, the search is initialized with an estimate that D_{eff} falls within the range of $[1\cdot10^{-9}, 1\cdot10^{-5}]\ cm^2/s$. This estimate stems from (a) the free-diffusion equation placing D_{free} at $1.067\cdot10^{-6}\ cm^2/s$, and, (b) a study that suggests that the D_{eff} at $7.8\cdot10^{-8}\ cm^2/s$ [12].

5 RESULTS AND DISCUSSION

The search algorithm converges on a value of $1.566\cdot10^{-7}\ cm^2/s$ for the effective diffusion coefficient for verapamil, with a minimum value of the L_2-norm of $0.145\ mg/mL$. However, plotting the concentration distribution resulting from free and two-compartment diffusion models, one notes a significant dissimilarity in the spatial variation of the solution. Take for example the solution space at time, $t = 1\,hr$.

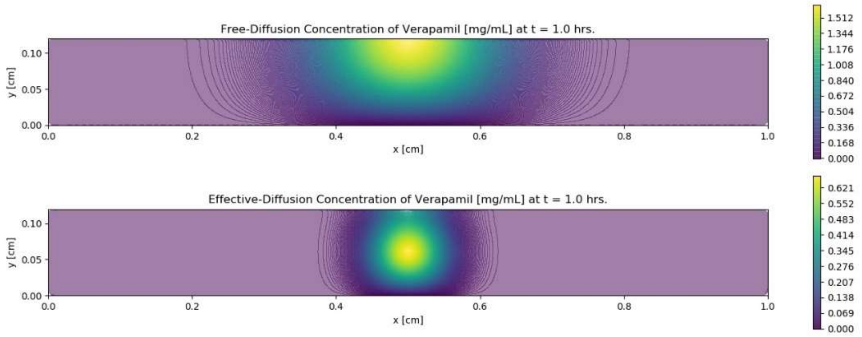

Figure 5: Free-Diffusion versus Effective Diffusion for Verapamil at t = 1 hr.; $D_{eff} = 1.566 \cdot 10^{-7} \ \ cm^2 / s$

It appears that the diffusion coefficient is *significantly* smaller than it should be. To understand what is happening, we also produce a solution of a higher effective-diffusion coefficient, one that more closely approximates the observed spatial distribution from the free-diffusion model. This field solution was generated with an effective-diffusion coefficient of $10.001 \cdot 10^{-7} \ \ cm^2 / s$ and returns an L_2-norm of $0.159 \ \ mg / mL$.

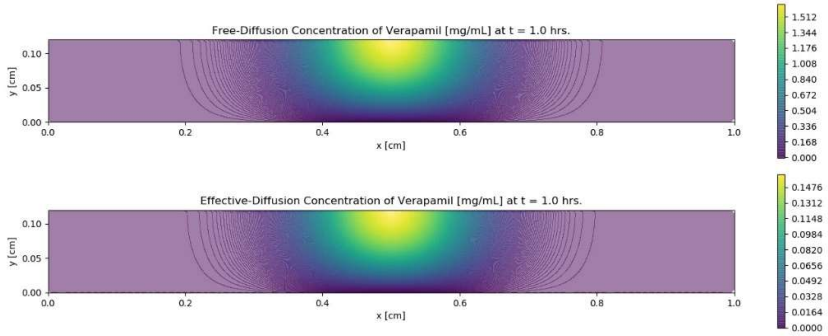

Figure 6: Free-Diffusion versus Effective Diffusion for Verapamil at t = 1 hr.; $D_{eff} = 10.001 \cdot 10^{-7} \ \ cm^2 / s$

Observing the scale of the solutions in Figure 6, one notes that the scale of the effective-diffusion solution is approximately one order-of-magnitude smaller than that of the free-diffusion solution. Recall that all the above solutions begin with the same initial mass of verapamil within the domain. The differences in the field solution arise from the elimination effects, which impose the removal of verapamil mass from the domain and which were ignored in the free-diffusion model. In the free-diffusion model, mass only exits the domain at the sink condition imposed at the lower boundary.

Whereas, in Figure 5, the scale of the effective-diffusion solution is much closer to that of the free-diffusion solution. Thus, it can be inferred that the Golden Section Search is electing to minimize the effective-diffusion coefficient in order to minimize the quantity of verapamil escaping the domain at the sink boundary. This makes sense; given that the fitness/objective function is defined explicitly using the compound concentration. For future work, it would

then be imperative to consider the flux of the solution as part of the fitness of the design parameters. However, this might lead to competing objectives between the two aspects of the fitness definition.

6 CONCLUSION

The LCMM provides an efficient methodology for the solution of the governing equations at hand. The search algorithm is likewise efficient, given the lack of a direct functional relationship between the design parameters and the objective function. Also, it appears that the search algorithm is conducting its search as specified, however, in a roundabout, rather unanticipated manner. A future implementation would require incorporation of the flux of the field solution in the objective function in order to more accurately represent the spatial distribution of the concentration.

Given the larger effective-diffusion coefficient, $D_{eff} = 10.001 \cdot 10^{-7}\ cm^2/s$, the spatial variation of the effective-diffusion model does appear to very closely approximate that of the free-diffusion model. However, it is important to note the scale of the solution is off by approximately one order of magnitude. This, of course, is a consequence of the elimination considerations. The effective-diffusion model allows for metabolism and elimination effects, which allows for mass to leave the domain, whereas it would otherwise be contained within the domain free-diffusion model, excluding that which is lost at the boundaries.

Thus, it is apparent from the results of the analysis that the free-diffusion model cannot approximate the solution of the total-diffusion model accurately without properly accounting for elimination effects. Metabolism and elimination allow for large quantities of the compound to exit the domain, significantly impacting the distribution accuracy of the field solution. It may be of possible to include a first-order elimination coefficient that accounts for both metabolic elimination in the tissue compartment and capillary clearance in the blood compartment, as a single term in sort of modified free-diffusion model. While this may seem to be regressing to a time before multi-compartment models, the ability to account for effects from multiple compartments using only the measurements from a single compartment may provide a step forward in the field of inverse problems for transdermal drug delivery.

REFERENCES

[1] de Monte F, Pontrelli G, Becker SM. “Transdermal Drug Delivery and Percutaneous Absorption,” *Heat Transfer and Fluid Flow in Biological Processes*, (2015), 273–304.

[2] Nitsche JM, Frederick Frasch H. Dynamics of diffusion with reversible binding in microscopically heterogeneous membranes: General theory and applications to dermal penetration. *Chem. Eng. Sci.* (2011) **66**:2019–41.

[3] Anissimov YG, Jepps OG, Dancik Y, Roberts MS. Mathematical and pharmacokinetic modelling of epidermal and dermal transport processes. *Adv. Drug Deliv. Rev.* (2013) **65**:169–90.

[4] Kretsos K, Kasting GB. Dermal capillary clearance: Physiology and modeling. *Skin Pharmacol. Physiol.* (2005) **18**:55–74.

[5] Kretsos K, Miller MA, Zamora-Estrada G, Kasting GB. Partitioning, diffusivity and clearance of skin permeants in mammalian dermis. *Int. J. Pharm.* (2008) **346**:64–79.

[6] Gray H. “The Common Integument,” In: Lewis WH, editor., *Anatomy of the Human*

Body, (1986), 1396, 20th ed.

[7] Yamaguchi K, Morita K, Mitsui T, Aso Y, Sugibayashi K. Skin permeation and metabolism of a new antipsoriatic vitamin D3 analogue of structure 16-en-22-oxa-24-carboalkoxide with low calcemic effect. *Int. J. Pharm.* (2008) **353**:105–12.

[8] Tojo K. Mathematical Modeling of Transdermal Drug Delivery. *J. Chem. Eng. Japan* (1987) **20**:301–8.

[9] Liu X, Yousef S, Anissimov YG, van der Hoek J, Tsakalozou E, Ni Z, et al. Diffusion modelling of percutaneous absorption kinetics. Predicting urinary excretion from in vitro skin permeation tests (IVPT) for an infinite dose. *Eur. J. Pharm. Biopharm.* (2020) **149**:30–44.

[10] Naegel A, Heisig M, Wittum G. Detailed modeling of skin penetration-An overview. *Adv. Drug Deliv. Rev.* (2013) **65**:191–207.

[11] Amarah AA, Petlin DG, Grice JE, Hadgraft J, Roberts MS, Anissimov YG. Compartmental modeling of skin transport. *Eur. J. Pharm. Biopharm.* (2018) **130**:336–44.

[12] Al-Qallaf B, Mori D, Olatunji L, Bhusan Das D, Cui Z, Das DB, et al. Transdermal drug delivery by microneedles: does skin metabolism matter? *Int. J. Chem. React. Eng.* (2009) **7**:1–23.

[13] Hikima T, Tojo K, Maibach HI. Skin metabolism in transdermal therapeutic systems. *Skin Pharmacol. Physiol.* (2005) **18**:153–9.

[14] Anissimov YG, Roberts MS. Modelling dermal drug distribution after topical application in human. *Pharm. Res.* (2011) **28**:2119–29.

[15] Grassi M, Lamberti G, Cascone S, Grassi G. Mathematical modeling of simultaneous drug release and in vivo absorption. *Int. J. Pharm.* (2011) **418**:130–41.

[16] Anissimov YG, Roberts MS. Diffusion modelling of percutaneous absorption kinetics: 4. Effects of a slow equilibration process within stratum corneum on absorption and desorption kinetics. *J. Pharm. Sci.* (2009) **98**:772–81.

[17] Tojo K, Chiang CC, Chien YW. Drug permeation across the skin: Effect of penetrant hydrophilicity. *J. Pharm. Sci.* (1987) **76**:123–6.

[18] Sarra SA, Kansa EJ. Multiquadric radial basis function approximation methods for the numerical solution of partial differential equations. *Adv. Comput. Mech.* (2009) **2**:2009.

[19] Madych WR. Miscellaneous error bounds for multiquadric and related interpolators. *Comput. Math. with Appl.* (1992) **24**:121–38.

[20] Franke R. A Critical Comparison of Some Methods for Interpolation of Scattered Data 1979.

[21] Li J, Cheng AHD, Chen CS. A comparison of efficiency and error convergence of multiquadric collocation method and finite element method. *Eng. Anal. Bound. Elem.* (2003) **27**:251–7.

[22] Cheng AHD, Golberg MA, Kansa EJ, Zammito Q. Exponential convergence and H-c multiquadric collocation method for partial differential equations. *Numer. Methods Partial Differ. Equ.* (2003) **19**:571–94.

[23] Imazawa R, Kawano Y, Itami K. Meshless method for solving fixed boundary problem of plasma equilibrium. *J. Comput. Phys.* (2015) **292**:208–14.

[24] Divo E, Kassab AJ. An efficient localized radial basis function meshless method for fluid flow and conjugate heat transfer. *J. Heat Transfer* (2007) **129**:124–36.

[25] Erhart K, Divo E, Kassab A. An evolutionary-based inverse approach for the identification of non-linear heat generation rates in living tissues using a localized meshless method. *Int. J. Numer. Methods Heat Fluid Flow* (2008) **18**:401–14.
[26] Khoury A, Divo E, Kassab A, Kakuturu S, Reddi L. Meshless modeling of flow dispersion and progressive piping in poroelastic levees. *Fluids* (2019) **4**:1–22.
[27] Cheng AHD. Multiquadric and its shape parameter - A numerical investigation of error estimate, condition number, and round-off error by arbitrary precision computation. *Eng. Anal. Bound. Elem.* (2012) **36**:220–39.
[28] Buhmann MD, Levesley J. Radial Basis Functions: Theory and Implementations. *Math. Comput.* (2004) **73**:1578–81.
[29] Kansa EJ, Holoborodko P. On the ill-conditioned nature of C∞ RBF strong collocation. *Eng. Anal. Bound. Elem.* (2017) **78**:26–30.
[30] Kansa EJ, Hon YC. Circumventing the Ill-conditioning problem with multiquadric radial basis functions: applications to elliptic partial differential equations. *Comput. Math. with Appl.* (2000) **39**:123–37.
[31] Ling L, Kansa EJ. A least-squares preconditioner for radial basis functions collocation methods. *Adv. Comput. Math.* (2005) **23**:31–54.
[32] Yao G, Siraj-Ul-Islam, Šarler B. Assessment of global and local meshless methods based on collocation with radial basis functions for parabolic partial differential equations in three dimensions. *Eng. Anal. Bound. Elem.* (2012) **36**:1640–8.
[33] Boyd JP. "Chebyshev & Fourier Series," *Chebyshev and Fourier Spectral Methods*, (2000), 19–60, 2nd ed.
[34] Anderson P, Bondesson U, Sylvén C. Clinical pharmacokinetics of verapamil in patients with atrial fibrillation. *Eur. J. Clin. Pharmacol.* (1982) **23**:49–57.
[35] Eichelbaum M, Somogyi A, von Unruh GE, Dengler HJ. Simultaneous determination of the intravenous and oral pharmacokinetic parameters of D,L-verapamil using stable isotope-labelled verapamil. *Eur. J. Clin. Pharmacol.* (1981) **19**:133–7.
[36] Koike Y, Shimamura K, Shudo I, Saito H. Pharmacokinetics of verapamil in man. *Res. Commun. Chem. Pathol. Pharmacol.* (1979) **24**:37–47.
[37] Chopra K, Calva D, Sosin M, Tadisina KK, Banda A, De La Cruz C, et al. A comprehensive examination of topographic thickness of skin in the human face. *Aesthetic Surg. J.* (2015) **35**:1007–13.
[38] Divo E, Kassab A, Rodriguez F. Characterization of space dependent thermal conductivity with a bem-based genetic algorithm. *Numer. Heat Transf. Part A Appl.* (2000) **37**:845–75.
[39] Kiefer J. Sequential Minimax Search for a Maximum. *Proc. Am. Math. Soc.* (1953) **4**:502.